SENSORLESS CONTROL OF A PERMANENT MAGNET SYNCHRONOUS MOTOR FOR PV-POWERED WATER PUMP SYSTEMS USING THE EXTENDED KALMAN FILTER

G. Terörde, K. Hameyer and R. Belmans

Katholieke Universiteit Leuven, Belgium

ABSTRACT: The system studied in this paper is a sensorless control of a permanent magnet synchronous motor (PMSM). Its structure is based on the extended Kalman filter theory using only the measurement of the motor current for the on-line estimation of speed and rotor position. The PMSM, driving a water pump, is supplied by a PV array. The implemented PV array is designed for a peak power of 1,2 kW. To search the maximum power point (MPP) of the PV array, the inverter is operated with variable frequency adapting the power input of the motor. The PWM generation is done by space vector modulation. The motor voltages necessary for the Kalman algorithm are calculated considering the non-linearity of the inverter. The main control is done by a TMS320C31 DSP. The I/O subsystem and the PWM generation are based on a TMS320P14 working as a slave-DSP. Finally, an evaluation of the experimental results is presented.
Keyword: Machines in renewable energy systems

1. INTRODUCTION

The entire control system, studied in this paper, is shown in figure 1. The inverter operates as a variable frequency source (PWM) for the PMSM driving the pump. Since a PMSM in open-loop is unstable, a vector control with feedback of speed and position, estimated by an extended Kalman filter, is proposed. Furthermore, the inverter is equipped with a maximum power point tracker (MPPT).

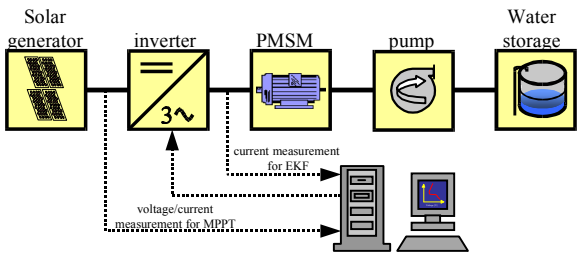

Figure 1: Block diagram of the analysed system.

Most PV powered water pump systems consist of a control unit, with or without battery as energy storage. The MPPT is controlled by varying the duty ratio of a DC-DC converter. Using this converter leads to a less complicated control algorithm for the MPPT. On the other hand, this converter introduces losses, such as switching losses, valve losses and copper and iron losses in the filter coil. In control systems without a battery, the DC bus may collapse when an unbalanced input/output power ratio occures at the DC bus.
The system analysed here is a water pumping system avoiding the use of the additional DC-DC converter, a battery and its losses. Because of the lack of a storage in the DC bus, the power of the PV array must be used immediately to accelerate the PMSM. As the irradiance increases, resulting in a higher output power of the PV array, the input power in the DC bus is higher than the output power. The MPP control must immediately accelerate the PMSM to track the MPP of the PV array. With decreasing illumination, the power of the PV array is smaller than the output power in the DC bus. This is the most critical condition of the system. The DC bus may collapse, if this condition continues. Hence, the inverter must slow down the PMSM. Therefore, the controller should guarantee a balanced input/output power ratio in the DC bus. To optimise the energy captured by the PV array, the output power should always be at its maximum. The output power of the PMSM can be controlled by varying the speed of the motor and the pump respectively.

2. MOTOR MODEL

The Kalman filter is based on a machine model of the permanent magnet synchronous motor (PMSM) in (discrete-time) state space. The dynamic model for the PMSM in a stator-fixed reference frame (indices: '^{s}'), choosing the rotor-fixed current i_d, i_q, the angular velocity ω_e, and the rotor position γ as state variable $\underline{x}_k$ and the fundamental voltage as input $\underline{u}_k$, is described by equations (1)-(4). This model assumes the velocity ω_e to be constant in a small time interval (sampling time T_s).

$$\underline{x}_{k+1} = \underline{A}(\underline{x}_k)\cdot\underline{x}_k + \underline{B}(\underline{x}_k)\cdot\underline{u}_k\,,\ \underline{x}_k = \begin{pmatrix} i_d \\ i_q \\ \omega_e \\ \gamma \end{pmatrix}_k,\ \underline{u}_k = \begin{pmatrix} U_d^s \\ U_q^s \end{pmatrix}_k \quad (1)$$

$$\underline{A}(\underline{x}_k) = \begin{pmatrix} 1-R_1\frac{T_s}{L_d} & \omega_e T_s\frac{L_q}{L_d} & 0 & 0 \\ -\omega_e T_s\frac{L_d}{L_q} & 1-R_1\frac{T_s}{L_q} & -T_s\frac{\Psi}{L_q} & 0 \\ 0 & 0 & 1 & 0 \\ 0 & 0 & T_s & 1 \end{pmatrix} \quad (2)$$

$$\underline{B}(\underline{x}_k) = \begin{pmatrix} T_s \dfrac{\cos(\gamma)}{L_d} & T_s \dfrac{\sin(\gamma)}{L_d} \\ -T_s \dfrac{\sin(\gamma)}{L_q} & T_s \dfrac{\cos(\gamma)}{L_q} \\ 0 & 0 \\ 0 & 0 \end{pmatrix} \qquad (3)$$

with: R_1 = resistance, $L_{d/q}$ = d/q axis inductance, ψ = permanent magnet flux linkage.

The resulting output vector $\underline{y}_k$ consists of the estimated motor current in a stator-fixed reference frame being compared to the measured current. The difference is used to correct the state vector of the system model.

$$\underline{y}_k = \begin{pmatrix} I_d^s(k) \\ I_q^s(k) \end{pmatrix} = \begin{pmatrix} \cos(\gamma) & -\sin(\gamma) & 0 & 0 \\ \sin(\gamma) & \cos(\gamma) & 0 & 0 \end{pmatrix} \underline{x}_k \qquad (4)$$

A block diagram of the discrete motor model and extended Kalman filter is shown in figure 2.

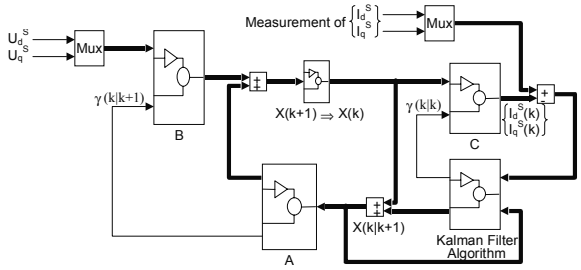

Figure 2: Block diagram of the discrete motor model and extended Kalman filter.

3. PHASE VOLTAGE

The extended Kalman filter algorithm requires the motor voltages as input quantities. An alternative to the complex measurement and filtering of the motor voltage is the use of the reference voltage for the PWM, available at the output of the current control. The PWM generation is performed by space vector modulation (SVM). The SVM minimizes the harmonic content, determining the copper losses of the machine, accounting for a major portion of the machine losses. SVM also provides a more efficient use of the supply voltage in comparison to sinusoidal modulation methods. The homopolar system containing in the phase voltages, must be considered in the Park transformation. In case of an ideal inverter, the filtered phase voltage U assumes the shape of the reference voltage U_{ref}. Due to the delayed reacting of almost all semiconductor switches at turn-on and turn-off, the phase voltages strongly deviate from the reference voltages. This leads in the Kalman filter algorithm to large position and speed errors. At low motor speed the control becomes even unstable. With positive current the duty cycles are shorter, with negative current they are longer than required. Hence, the actual duty cycle of a bridge is always different from that of the reference voltage. It is either increased or decreased, depending on the load current polarity. This effect is described by an error voltage ΔU

$$\Delta U \approx \frac{U_T + U_D}{2} + t_d \cdot f_{PWM} \cdot U_c \qquad (5)$$

dependent on the dead-time t_d, the DC-bus voltage U_c, the PWM-frequency f_{PWM} and the voltages U_D and U_T at transistor and diode [2]. These voltage values and the resistances R_T and R_D of the switch change the inverter output from its intended value U_{ref} to

$$U \approx U_{ref} - I \cdot \frac{R_{T1} + R_D}{2} - \Delta U \cdot \mathrm{sign}(I)\,, \qquad (6)$$

used as input of the Kalman filter.

4. EXTENDED KALMAN FILTER ALGORITHM

The state model of the PMSM is non-linear. The electrical speed and the position of the rotor are considered as both, state and parameter. The model matrices $\underline{B}$ and $\underline{C}$ depend on the position of the rotor, the matrix $\underline{A}$ on the electrical speed. Therefore, the extended Kalman filter (EKF) has to be used to estimate the parameters of the model matrices, as well. The EKF re-linearises the non-linear state model for each new estimation step, as it becomes available. Furthermore, the EKF provides a solution that directly cares for the effects of measurement or system noises. The errors in the parameters of the system model are also handled as system noise. The used algorithm of the EKF is based on Brammer [3]. The signal flow of the EKF in a recursive manner is shown in figure 3.

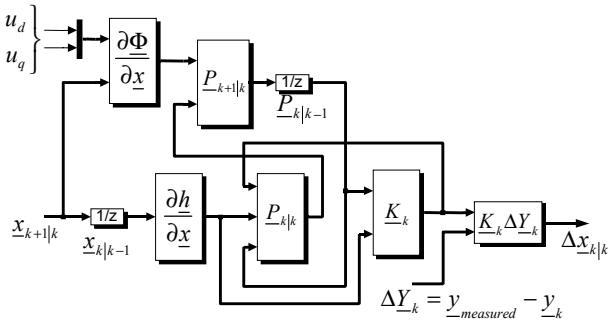

Figure 3: Block diagram of the extended Kalman filter

It has to be distinguished between the filter and predictor equations. The predicted value of the state vector $\underline{x}_{k+1|k}$ is corrected by multiplying the filter gain and the difference between estimated and measured output vector $\underline{y}_k$ to the state vector $\underline{x}_{k|k}$. In addition still

the equation for the corrected covarianz matrix $\underline{P}_{k|k}$ is required.

$$\underline{x}_{k|k} = \underline{x}_{k|k-1} + \underline{K}_k \left(\underline{y}_k - \underline{h}\left(\underline{x}_{k|k-1}, k\right) \right) \tag{7}$$

$$\underline{P}_{k|k} = \underline{P}_{k|k-1} - \underline{K}_k \frac{\partial \underline{h}}{\partial \underline{x}} |_{\underline{x}=\underline{x}_{k|k-1}} \underline{P}_{k|k-1} \tag{8}$$

The matrix $\underline{K}_k$ is the feedback matrix of the extended Kalman filter (EKF). This matrix determines how the state vector $\underline{x}_{k|k}$ is modified after the output of the model $\underline{y}_k$ is compared to the measured output of the system. The filter gain matrix is defined by:

$$\underline{K}_k = \underline{P}_{k|k-1} \frac{\partial \underline{h}^T}{\partial \underline{x}} |_{\underline{x}=\underline{x}_{k|k-1}} \left(\frac{\partial \underline{h}}{\partial \underline{x}} |_{\underline{x}=\underline{x}_{k|k-1}} \underline{P}_{k|k-1} \frac{\partial \underline{h}^T}{\partial \underline{x}} |_{\underline{x}=\underline{x}_{k|k-1}} + \underline{R} \right)^{-1} \tag{9}$$

in which $\underline{R}$ is based on the covariance matrix of the measurement noise.
Based on the calculated state vector $\underline{x}_{k|k}$, a new value of the state vector can be predicted. The same applies to the error covariance matrix. The prediction is given by

$$\underline{x}_{k+1|k} = \underline{\Phi}\left(k+1, k, \underline{x}_{k|k-1}, \underline{u}_k\right) \tag{10}$$

$$\underline{P}_{k+1|k} = \frac{\partial \underline{\Phi}}{\partial \underline{x}} |_{\underline{x}=\underline{x}_{k|k}} \underline{P}_{k|k} \frac{\partial \underline{\Phi}^T}{\partial \underline{x}} |_{\underline{x}=\underline{x}_{k|k}} + \underline{\Gamma}_k \underline{Q} \underline{\Gamma}_k^T \tag{11}$$

with the covariance matrix $\underline{Q}$ of the system noise. The system vector $\underline{\Phi}$ and the output vector $\underline{h}$ respectively can be derived from the model equations of the PMSM.

$$\underline{\Phi}\left(k+1, k, \underline{x}_{k|k-1}, \underline{u}_k\right) = \underline{A}_k\left(\underline{x}_{k|k}\right)\underline{x}_{k|k} + \underline{B}_k\left(\underline{x}_{k|k}\right)\underline{u}_{k|k} \tag{12}$$

$$\underline{h}\left(\underline{x}_{k|k-1}, k\right) = \underline{C}_k\left(\underline{x}_{k|k-1}\right)\underline{x}_{k|k-1} \tag{13}$$

$$\frac{\partial \underline{h}}{\partial \underline{x}} = \begin{pmatrix} \cos(\gamma) & -\sin(\gamma) & 0 & -i_d \sin(\gamma) - i_q \cos(\gamma) \\ \sin(\gamma) & \cos(\gamma) & 0 & i_d \cos(\gamma) - i_q \sin(\gamma) \end{pmatrix} \tag{14}$$

$$\frac{\partial \underline{\Phi}}{\partial \underline{x}} = \begin{pmatrix} 1 - R_1 \frac{T_s}{L_d} & \omega_e T_s \frac{L_q}{L_d} & T_s \frac{L_q}{L_d} i_q & \frac{T_s}{L_d} u_q \\ -\omega_e T_s \frac{L_d}{L_q} & 1 - R_1 \frac{T_s}{L_q} & -\frac{T_s}{L_q}\left(L_d i_d + \Psi\right) & -\frac{T_s}{L_q} u_d \\ 0 & 0 & 1 & 0 \\ 0 & 0 & T_s & 1 \end{pmatrix} \tag{15}$$

where u_q and u_d are voltages in a rotor-fixed reference frame.
The critical step in the EKF is the search for the best covariance matrices. $\underline{Q}$ and $\underline{R}$ have to be set-up based on the stochastic properties of the corresponding noise. The noise covariance $\underline{R}$ accounts for the measurement noise introduced by the current sensors and the quantization errors of the A/D converters. Increasing $\underline{R}$ indicates stronger disturbance of the current. The noise is weighted less by the filter, causing also a slower transient performance of the system. The noise covariance $\underline{Q}$ reflects the system model inaccuracy, the errors of the parameters and the noise introduced by the voltage estimation. $\underline{Q}$ has to be increased at stronger noise driving the system, entailing a more heavily weighting of the measured current and a faster transient performance. An initial matrix $\underline{P}_0$ represents the matrix of the covariance in knowledge of the initial conditions. Varying $\underline{P}_0$ affects neither the transient performance nor the steady state conditions of the system.
In general, the entries of the covariance matrices $\underline{Q}$ and $\underline{R}$ are unknown and can not be calculated. They are often set equal to the unit matrix. In order to achieve a good filter performance, they must be filled based on experimental investigations. This describes an iterative process of searching the best values. In the following experiments, the best filter performance was obtained with:

$$\underline{R} = \mathbf{I};\ Q_{11} = Q_{22} = Q_{33} = 0.03;\ Q_{44} = 7 \cdot 10^{-5};\ \underline{P}_0 = 0.02 \cdot \mathbf{I}$$

whereby $\mathbf{I}$ is the identity matrix. $\underline{Q}$, $\underline{R}$ and $\underline{P}_0$ are assumed to be diagonal matrices.

5. EXPERIMENTAL RESULTS OF THE EKF

The execution time of the entire control system, including motor control, MPPT and EKF, amounts to 274 µs and the used sample time is T_s =300 µs. Figure 4 shows the experimental result of a speed reversal using the estimated speed and position as feedback. Additionally, the real speed and position are measured and compared.

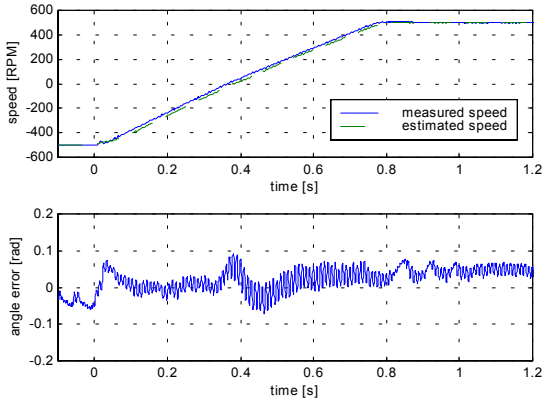

Figure 4: Speed reversal test. Above: Measured and estimated speed. Below: Error of the angle estimation.

It can be seen that there is a very good coincidence between real and estimated speed and position respectively. Figure 5 presents the response of the PMSM to a load step at a motor speed of 1000 RPM. The applied load amounts to 70% of the rated torque.

The current controller, using also the estimated values of d- and q-axis current, has a bandwidth of 926 Hz.

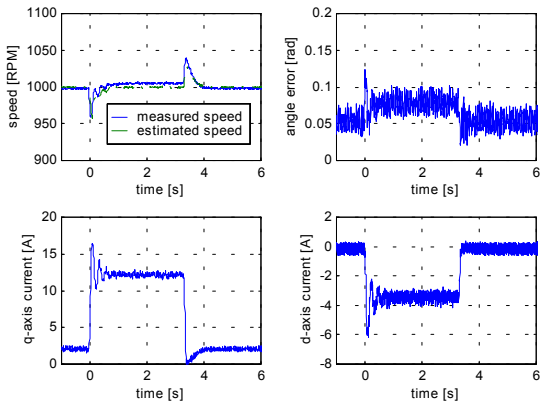

Figure 5: Load step (70% of the rated torque). Above: Speed and angle error. Below: estimated d/q- current.

The load disturbance creates a small speed error of 0.5%. This error is caused by the voltage estimation, depending on the dead-time and resistances of the switches. The steady state error can be further reduced by generating an offset for the speed reference using the frequency of the measured current. The angle error is negligible.

At low motor speed ($\omega \Rightarrow 0$) the equations of the PMSM are simplified as the voltage induced by the magnets is very small. Thus, no more predication can be made on the position of the magnets and the EKF fails. Since at standstill only DC-values are given, the necessary flux variation must be forced by impressing a test signal into the system. A signal, which can be implemented easily, represents an additional sinusoidal reference current in the d-axis of the motor, using the d/q axis-symmetrie of the rotor to estimate the real position. In all presented experimental results the following d-axis reference current is used:

$$i_{d,ref} = i_d^* + 5\text{A}\sin(2\pi\, 200\frac{1}{\text{s}}t)\cdot\left(1-\frac{|n|}{500\text{RPM}}\right) \qquad (16)$$

whereby i_d^* results from the speed control. The generated reluctance torque is compensated by a complementary q-axis current. The electromagnetic torque T_e can be expressed as:

$$T_e = p\left[\Psi\, i_q - (L_q - L_d)\, i_d\, i_q\right] \qquad (17)$$

The optimal control of the motor takes advantage of the reluctance torque by introducing a negative ($L_d < L_q$) direct axis current component. In figure 6 a comparison is given of motor control with feedback of the estimated speed and optimum d-axis current, motor control with feedback of the estimated speed and no d-axis current and motor control with feedback of the measured speed and position (FOC).

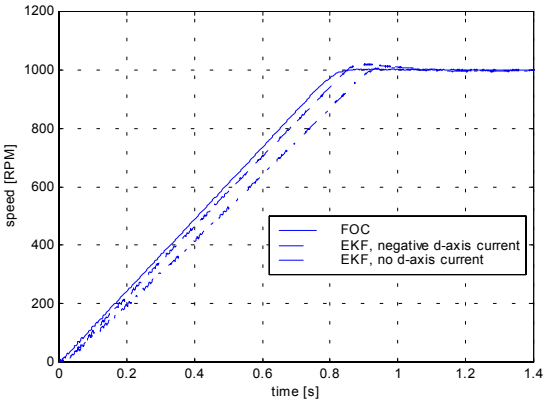

Figure 6: Speed step with feedback of the estimated speed and position (EKF), optimum d-axis current, no d-axis current and with feedback of the measured speed and position (FOC).

6. MPP-TRACKING

The efficiency of the output power of a PV array can be increased about 2% by MPP-Tracking, compared to a common constant voltage tracking. The Maximum Power Point (MPP) is characterised by the voltage, where the PV array generates maximum output power. The practically studied PV array consists of 11 modules in series with a total peak power of 1,2 kW. The characteristics of the PV elements are affected by the irradiance and the cell temperature. To reach the point of maximum power at rising irradiance, the current in the DC bus must be increased while the DC voltage remains nearly constant. The voltage at the MPP changes with the array temperature and the current is almost unaffected. At lower cell temperature the MPP characteristic is situated in a higher voltage range. Thus, the optimum output voltage of the PV array is not constant and moves as the conditions vary. In contrast with the very fast and frequently changing irradiance, the cell temperature of the PV array and thus the DC voltage in the MPP varies very slowly. Therefore, MPPT is performed by varying the DC voltage in a small range, searching the MPP and controlling the speed of the PMSM in order to guarantee the calculated optimum voltage.

The overall control of the MPPT consists of a current controller, a speed controller and a main control for MPPT. The inner control varies the speed of the PMSM to stay in the calculated optimum voltage range. The input of this inner control is the voltage error, calculated from the measured and filtered DC voltage and the reference voltage given by the main control loop. The error voltage of this inner control loop is presented in figure 7. The averaged voltage error of the inner control loop is smaller than 0.1%. Also at the starting procedure and under very quickly changing irradiance (≈600 W/s) the error reaches a maximum of 0.5%. The averaged voltage error delivers the minimum search range for the

main control calculating the MPP. The inner control loop is done by a common PI controller with anti-windup.

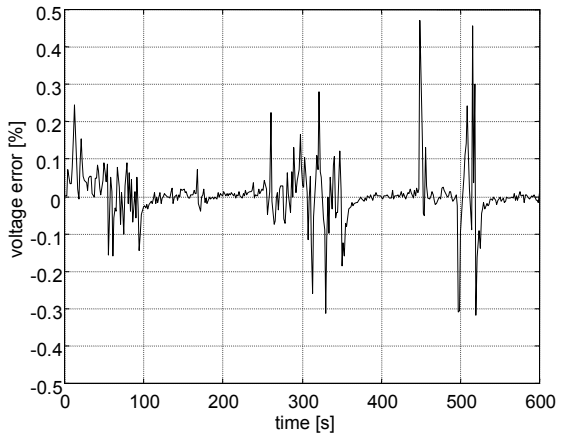

Figure 7: Voltage error of the inner control loop.

The main control loop calculates the MPP and the search range of the DC voltage and delivers the reference quantity of the inner control loop. First, a default voltage and search range must be given. After the default voltage is reached, the voltage is varied around this point. The quantity of the variation is given by the search range. During this variation, the power generated by the PV array is measured and the voltage linked with the maximum power is stored during the respective searching procedure. The new optimum voltage and the new search range are calculated from these actual measurements and in its history stored values by an adaptive controller. With these quantities the controller starts a new searching procedure to find the MPP.

The previous values are very important for the calculation of the new optimum voltage and search range. If, e.g., the new calculated optimum voltage during a searching procedure with rising voltage is situated higher than the last optimum voltage, the MPP-voltage seems to change. But this can also indicate an increasing irradiance. If the second condition occurs, the controller should not change the new optimum voltage. Otherwise, the calculated voltage drifts away from the MPP. The same considerations are also valid for a decreasing irradiance. Thus, the adaptive control must be able to distinguish between a changing MPP and changing conditions, respectively. The search range depends on the variation of the calculated optimum voltage. If the calculated MPP is situated in the half of the past voltage range, the search range is reduced, otherwise it is increased.

Measurements of the implemented MPPT are plotted in figure 3 showing the power of the PV array as a function of the DC voltage. Four different starting conditions (a-d) are shown to demonstrate the ability of reproduction of the MPPT. The characteristic c and d exhibit the MPPT starting with an unbalanced input/output power ratio on the DC bus. The MPP-voltage at characteristic a is situated in a higher voltage range, because it shows the first searching procedure at a lower array temperature.

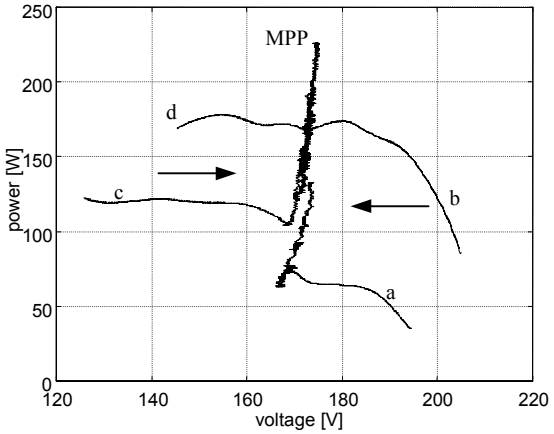

Figure 8: Measured results of MPPT (6 hours).

7. CONCLUSION

This paper presentes the design and the implementation for a sensorless speed control of a PMSM using the extended Kalman filter. Measurement and filtering of the motor voltages are not required. Instead, the reference voltages for the PWM are used for the DSP-based control. Results of the dynamic and steady state behaviour of the extended Kalman filter are given. A MPPT control without using an additional DC-DC converter is explained. The implemented MPPT is realised by feeding back the DC voltage and current to the controller, adjusting the speed of the PMSM and keeping the system operating at its MPP. The measured results of the MPPT exhibit the ability of reproduction and the stability of the system.

ACKNOWLEDGEMENT

This research is supported by the Ministry of Economy of Flemish Region (IWT-Vliet). The authors are also grateful to the Belgian “Fonds voor Wetenschappelijk Onderzoek Vlaanderen” for its financial support and to the Interuniversity MicroElectronics Centre IMEC for its practical support of this work.

REFERENCES

[1] Rajashekara K S, Kawamura A, 1994, "Sensorless Control of Permanent Magnet AC Motors", IEEE IECON Proceedings, pp. 1589-1594.

[2] Bose B K, 1997, "Power Electronics and Variable Frequency Drives", IEEE Press, New York.

[3] Brammer, Siffling, 1994, “Kalman-Bucy Filter, Deterministische Beobachtung und stochastische Filterung” R. Oldenbourg Verlag München, Wien.

[4] Strejc V, 1980, "State space theory of discrete linear control", John Wiley & Sons.